*Original research article*

SCIENCE PROGRESS

Science Progress
2025, Vol. 108(4) 1–16

DOI: 10.1177/00368504251399597
journals.sagepub.com/home/sci

Sage

# Renal fibrosis assessment in chronic kidney disease: Exploring varied kidney regions with ultrasound-based radiomics analysis

**Ziman Chen[1], Yingli Wang[2] and Chaoqun Wu[3,4]**

## Abstract

**Objectives:** This study aimed to develop and compare radiomics signatures derived from different renal regions on ultrasound images to assess fibrosis severity in chronic kidney disease (CKD) patients.

**Methods:** A total of 146 CKD patients who underwent renal ultrasound and biopsy were enrolled. Radiomics features were extracted from the whole kidney, parenchyma, and mid-portion to generate region-specific signatures: radscore_whole, radscore_parenchyma, and radscore_mid-portion. Diagnostic performance in distinguishing mild from moderate-to-severe fibrosis was evaluated using receiver operating characteristic (ROC) curve analysis. Performance improvements were assessed via net reclassification improvement (NRI) and integrated discrimination improvement (IDI).

**Results:** The radscore_mid-portion displayed the highest discriminatory accuracy, yielding an area under the ROC curve (AUC) of 0.74 (95% CI: 0.65–0.82), which exceeded both the radscore_whole (AUC = 0.61, 95% CI: 0.51–0.70; $P = 0.035$) and radscore_parenchyma (AUC = 0.66, 95% CI: 0.56–0.74; $P = 0.181$). Reclassification analysis confirmed the added diagnostic value of the mid-portion signature, with significant

[1]Department of Health Technology and Informatics, The Hong Kong Polytechnic University, Kowloon, Hong Kong
[2]Ultrasound Department, EDAN Instruments, Inc., Shenzhen, China
[3]Department of Ultrasound, The Fifth Affiliated Hospital of Sun Yat-sen University, Zhuhai, China
[4]Department of Ultrasound, The First Affiliated Hospital of Wenzhou Medical University, Wenzhou, China

**Corresponding author:**
Ziman Chen, Department of Health Technology and Informatics, The Hong Kong Polytechnic University, Kowloon, Hong Kong.
Email: chenzm27@alumni.sysu.edu.cn

improvements compared with both the whole-kidney (NRI = 36.35%; IDI = 10.57%) and parenchyma signatures (NRI = 42.23%; IDI = 10.42%).
**Conclusions:** Radiomics signatures from different renal regions offer varying diagnostic utility. The mid-portion-based signature demonstrated improved performance and added value in identifying moderate-to-severe renal fibrosis in CKD patients.

**Keywords**
Chronic kidney disease, renal fibrosis, ultrasound, radiomics

## Introduction

In recent times, there has been a noteworthy upsurge in the global incidence and mortality rates associated with chronic kidney disease (CKD).[1–3] This rise in numbers poses a significant threat to both public health and national healthcare systems. Furthermore, end-stage kidney disease (ESKD), the most severe form of CKD, afflicts approximately 3 million individuals worldwide.[4] These patients require vital kidney replacement therapies such as dialysis or kidney transplantation for their survival. Regardless of the initial trigger or underlying disease, renal fibrosis serves as the common pathological pathway through which CKD progresses to ESKD.[5,6] The accurate and timely diagnosis and staging of renal fibrosis are of utmost importance to facilitate the organized management and intervention for CKD patients. This strategic approach ultimately contributes to a reduction in the prevalence of ESKD and helps alleviate the substantial burden on healthcare resources.

Renal biopsy serves as the established procedure for fibrosis assessment; however, its invasive nature impedes the ability to dynamically monitor evolving clinical conditions or facilitate longitudinal management follow-up.[7,8] Conventional ultrasound (US) is acknowledged for its radiation-free attributes, cost-effectiveness, and noninvasive features, rendering it the foremost imaging modality for CKD diagnosis.[9] It serves as the primary approach through which most instances of renal damage are detected. Nonetheless, it is pertinent to highlight that US parameters, encompassing both morphological and hemodynamic metrics, undergo significant alterations primarily during the stages of advanced or irreversible presentations of renal impairment.[10,11] Consequently, the disease might have already progressed to a later stage, exerting an unfavorable influence on therapeutic efficacy.

Within the context of noteworthy progress in artificial intelligence and data mining, a growing spectrum of image analysis methods is being employed in the domain of medical image processing and adjunctive diagnostics.[12–14] Leveraging the capabilities of machine and deep learning, radiomics emerges as a burgeoning imaging analysis approach aimed at attaining precise diagnoses and treatment strategies noninvasively.[15] This is accomplished by extracting high-throughput quantitative data from medical images, thus enabling the anticipation of intrinsic heterogeneity.[16] These insights play a pivotal role in

fortifying the processes of clinical decision-making. Previous studies have utilized radiomics technology to analyze renal US images, thereby facilitating the diagnosis of kidney damage and the evaluation of renal function.[17,18] These efforts have yielded promising results. A recent study has underscored the varying diagnostic efficacy of radiomics features extracted from distinct lesion regions within US images, encompassing intratumoral, peritumoral, and parenchymal regions, in distinguishing between benign and malignant breast lesions.[19] This prompts contemplation on whether radiomics features extracted from varying kidney regions within US images, encompassing the renal parenchyma, the entirety of the renal structure (including both parenchyma and the collecting system), and the mid-portion segment of the renal parenchyma, similarly exhibit divergent diagnostic potentials, which may contribute to the refinement and optimization of the radiomics analysis framework for renal US.

Hence, the present study aims to establish and compare radiomics signatures extracted from various kidney regions within US images to assess the severity of renal fibrosis in CKD patients.

## Materials and methods

### *Study population*

This prospective cross-sectional clinical study received approval from the Ethics Committee of the Fifth Affiliated Hospital of Sun Yat-sen University (protocol code: K09-1; approval date: May 2019) and adhered to the principles outlined in the Declaration of Helsinki. Prior to participation, all individuals provided their informed consent by signing the consent forms. All patient data were anonymized prior to analysis to ensure that individual participants could not be identified.

Patients who underwent both renal US examination and renal biopsy were recruited in this study, spanning from April 2019 to June 2022. Inclusion criteria consisted of: (1) patients diagnosed with CKD in accordance with the 2012 Kidney Disease: Improving Global Outcomes (KDIGO) guidelines[20]; (2) patients who had undergone renal US prior to the renal biopsy; and (3) patients scheduled for renal fibrosis staging subsequent to the renal biopsy. Exclusion criteria encompassed: (1) patients afflicted with multiple renal cysts, masses, hydronephrosis, or calculi that could potentially impede image processing and analysis; (2) patients with suboptimal image quality; (3) instances where US images failed to capture the entire kidney, particularly when there was edge shadowing at the kidney poles; and (4) cases where the biopsy specimen was deemed inadequate or insufficient for a comprehensive pathologic diagnosis.

The study workflow's comprehensive design is depicted in Figure 1 and supplementary material. This study was conducted in accordance with the STROBE guideline.[21]

### *US image acquisition and ROI segmentation*

The US examination was conducted using the Aixplorer US imaging system (SuperSonic Imagine, Aix-en-Provence, France) equipped with a convex broadband probe (SC6-1)

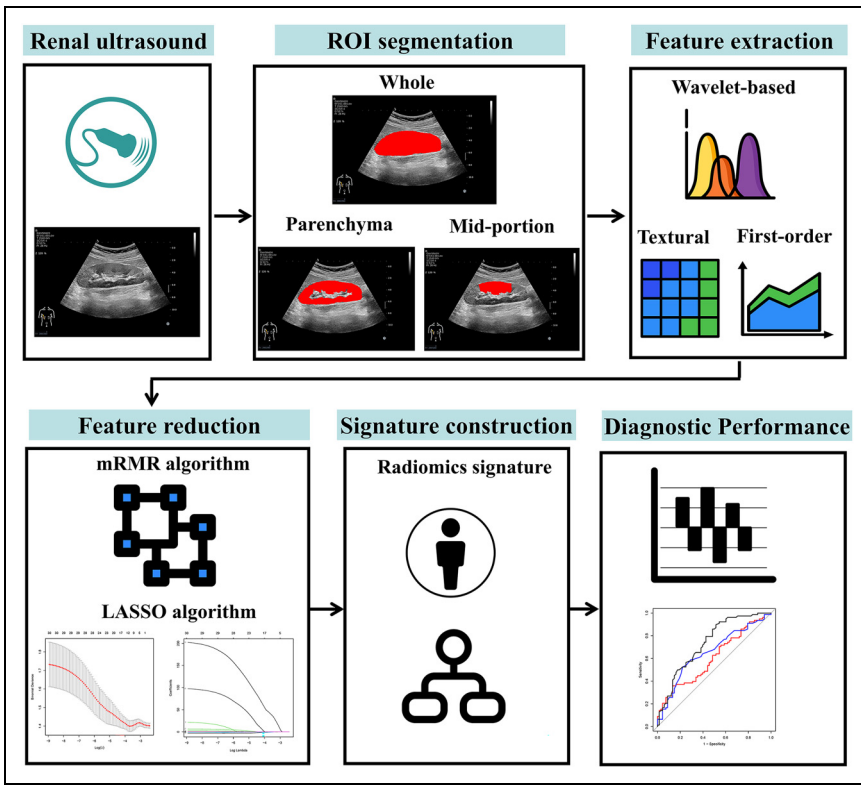


**Figure 1.** The flowchart of radiomics analyses.

operating at a frequency range of 1.0–6.0 MHz. An experienced, board-certified radiologist with 6 years of expertise in abdominal US performed all renal US examinations independently, within a two-day window preceding the renal biopsy. Throughout the examination, patients were positioned in a supine posture. Utilizing the B-mode US, the kidney was visualized through a longitudinal imaging approach, enabling the comprehensive depiction of its structures. The maximal coronal section of the right kidney was then precisely captured for subsequent analysis.

The regions of interest (ROI) were delineated in three distinct kidney regions: encompassing the entire kidney, the parenchyma alone, and the mid-portion. These delineations were performed manually by another radiologist with three years of experience in radiomics analysis. The radiologist, who remained uninformed about the fibrosis status of the patients, employed Microsoft Paint (Microsoft, Redmond, Washington, USA) to perform the ROI segmentations. For the whole kidney ROI, the delineation covered the entirety of the kidney, comprising both the parenchyma and the collecting system. The kidney parenchyma ROI focused solely on the parenchymal section of the kidney. Conversely, the kidney mid-portion ROI was

specifically confined to the central segment of the kidney. To ensure a standardized approach, the kidney length (from pole to pole) was divided into four equal parts and the two central segments were selected. These central segments were then projected onto the kidney parenchyma, effectively forming the mid-portion of the kidney. This definition was adopted to provide a reproducible method for localizing the ROI and to ensure a sufficiently large area for analysis while minimizing artifacts from the renal poles.

## Radiomics feature selection and signature construction

Radiomics features were extracted from the delineated ROIs using Pyradiomics (https://pyradiomics.readthedocs.io), an open-source Python package that provides standardized and reproducible extraction of quantitative imaging features, including intensity, texture, and wavelet-transformed features. All images were resampled to a pixel spacing of $1 \times 1\ mm^2$ with a fixed bin width of 25, and features were derived from both the original image and those processed with Laplacian of Gaussian (LoG) filtering (with sigma values of 3.0 and 4.0) as well as wavelet transformations.

A two-step feature selection strategy was then applied. First, the minimum redundancy maximum relevance (mRMR) algorithm was used to select features that were most strongly associated with the outcome while simultaneously reducing inter-feature redundancy. Second, least absolute shrinkage and selection operator (LASSO) regression with 10-fold cross-validation was employed. LASSO is a regularized regression method that shrinks the coefficients of less informative variables toward zero, thereby avoiding overfitting and yielding a stable and parsimonious set of predictors. Finally, a radiomics signature ("radscore") was calculated as a linear combination of the selected features weighted by their non-zero coefficients.

The procedures mentioned above were carried out individually within the whole kidney ROI, the renal parenchyma ROI, and the renal mid-portion ROI, respectively. The corresponding radiomics signatures were successfully established, namely radscore_whole, radscore_parenchyma, and radscore_mid-portion.

## Renal biopsy

Utilizing either a 16- or 18-gauge needle (Bard Magnum, Covington, GA, USA), a percutaneous renal biopsy was executed targeting the lower pole of the right kidney. Two pathologists, each possessing 6–8 years of expertise in nephropathology, independently scrutinized the pathological specimens, maintaining blindness to clinical information. Consensus was achieved by deliberative resolution of any divergent interpretations. The evaluation of renal fibrosis employed a semi-quantitative scoring system, in accordance with the methodology outlined in our preceding study.[22] The derived pathological scores facilitated the categorization of cases into the spectrum of mild, moderate, and severe fibrosis. Given the relatively limited occurrence of severe cases ($n = 16$), we consolidated the moderate and severe groups into a unified "moderate-to-severe" group for the purpose of comparison with the mild group.

### Statistical analysis

The statistical analysis was conducted through employing R software (version 4.2.1), Python software (version 3.11.4), and SPSS software (version 26.0; SPSS, Inc., Chicago, IL). Categorical variables were denoted in terms of counts (percentages), whereas continuous variables were depicted as mean ± standard deviation or median (interquartile range) as suitable. The receiver operating characteristic (ROC) curve was constructed to appraise the diagnostic performance of radiomics signature in the differentiation of renal fibrosis severity. Quantification of the extent of discriminative capability was executed by means of calculating the area under the ROC curve (AUC). The bootstrap resampling method, with 1000 iterations, was employed to compute the 95% confidence interval (CI) for the AUC value. The comparison of AUCs was carried out employing the DeLong test. Determination of sensitivity, specificity, and accuracy was accomplished through identification of the optimal threshold utilizing the Youden index. Utilization of the density map visually depicted the performance of the radiomics signature in discrimination. The internal validation of the radiomics signature was conducted using a five-fold cross-validation approach. Enhancement in the performance of specific regional radiomics signatures was quantified by evaluating net reclassification improvement (NRI) and integrated discrimination improvement (IDI). Statistical significance was set at a two-sided $P$-value of $< 0.05$.

## Results

### Baseline characteristics of study cohort

Finally, a total of 146 patients were included in the study. The patients in the mild group had an average age of $33.85 \pm 12.74$ years, with a gender distribution of 36 males and 32 females. In contrast, those in the moderate-to-severe group exhibited an average age of $45.17 \pm 14.06$ years, with a gender distribution of 43 males and 35 females. The mild group exhibited a higher average renal length compared to the moderate-to-severe group. Comprehensive patient information is provided in Table 1.

### Establishment of radiomics signature

In total, 651 radiomics features were extracted from the US images encompassing the entire renal region of each patient. These radiomics features underwent a rigorous selection process, ultimately identifying four fibrosis-related features for the whole kidney region through the application of both the mRMR and LASSO algorithms. Employing the same procedures, 651 radiomics features from the renal parenchymal region resulted in the retention of five fibrosis-related features, while the renal mid-portion region yielded 12 such features. Subsequently, three distinct radiomics signatures were constructed, each representing a different renal region. These signatures were formed by applying a linear combination of the aforementioned features, weighted by their corresponding LASSO coefficients. Further details regarding the radiomics signatures can be found in Table 2.

**Table 1.** Baseline characteristics of study cohort.

| Characteristic | Mild fibrosis ($n = 68$) | Moderate-to-severe fibrosis ($n = 78$) |
|---|---|---|
| Age (years) | 33.85 ± 12.74 | 45.17 ± 14.06 |
| Sex | | |
| Male | 36 (52.94) | 43 (55.13) |
| Female | 32 (47.06) | 35 (44.87) |
| eGFR (mL/min/1.73 $m^2$) | 105.29 ± 25.20 | 70.16 ± 32.64 |
| Renal length (cm) | 10.60 ± 0.79 | 10.32 ± 0.87 |
| Radscore_whole | 0.11 (0.02–0.14) | 0.12 (0.10–0.30) |
| Radscore_parenchyma | 0.06 (0.00–0.11) | 0.14 (0.05–0.27) |
| Radscore_mid-portion | -0.14 (-0.33–0.19) | 0.27 (-0.01–0.58) |

*Note:* Categorical variables are presented as *n* (%) and continuous variables as mean ± standard deviation or median (interquartile range).
eGFR: estimated glomerular filtration rate.

**Table 2.** Construction of radiomics signatures across diverse regions.

| Index | Formula |
|---|---|
| Radscore_whole | 0.169–0.473 × wavelet.LH_glrlm_GrayLevelNonUniformityNormalized<br>+0.108 × wavelet.LH_firstorder_Median<br>+0.0993 × wavelet.HL_firstorder_Mean<br>+5.193 × wavelet.LH_glcm_ClusterProminence |
| Radscore_parenchyma | −0.348 + 0.0000314 × original_glrlm_GrayLevelNonUniformity<br>+0.00447 × wavelet.HL_firstorder_Mean<br>−0.0000910 × wavelet.HL_glcm_Autocorrelation<br>−0.0000225 × wavelet.HL_glcm_ClusterProminence<br>−0.0000219 × wavelet.LH_glcm_ClusterProminence |
| Radscore_mid-portion | 0.369 + 0.0307 × log.sigma.3.0.mm.3D_ngtdm_Strength<br>−0.178 × wavelet.LH_glcm_Imc2<br>−0.00206 × wavelet.LL_firstorder_RobustMeanAbsoluteDeviation<br>+43.882 × wavelet.LH_glrlm_ShortRunLowGrayLevelEmphasis<br>+0.00198 × wavelet.LH_firstorder_MeanAbsoluteDeviation<br>+0.0123 × original_glcm_Contrast<br>−0.00816 × original_firstorder_Mean<br>+0.000428 × wavelet.LH_gldm_LargeDependenceHighGrayLevelEmphasis<br>−0.133 × wavelet.LL_glcm_JointEntropy<br>−0.908 × wavelet.HL_glcm_Imc2<br>+0.000690 × wavelet.HH_ngtdm_Complexity<br>+0.000241 × wavelet.LL_gldm_LargeDependenceHighGrayLevelEmphasis |

## *Diagnostic performance of radiomics signature*

The radscore_mid-portion demonstrated the highest discriminatory accuracy with an AUC value of 0.74 (95% CI: 0.65–0.82), surpassing both the radscore_whole (AUC = 0.61, 95% CI: 0.51–0.70; DeLong test: $P = 0.035$) and the radscore_parenchyma (AUC = 0.66, 95% CI: 0.56–0.74; DeLong test: $P = 0.181$) (Table 3, Figure 2). The

**Table 3.** Diagnostic performance of radiomics signatures across varied regions.

| Index | Sensitivity | Specificity | Accuracy | AUC (95% CI) | *P*-value[a] | *P*-value[b] |
|---|---|---|---|---|---|---|
| Radscore_whole | 0.69 | 0.46 | 0.58 | 0.61 (0.51–0.70) | — | — |
| Radscore_parenchyma | 0.64 | 0.60 | 0.62 | 0.66 (0.56–0.74) | 0.316 | — |
| Radscore_mid-portion | 0.86 | 0.51 | 0.70 | 0.74 (0.65–0.82) | 0.035 | 0.181 |

AUC: area under the curve; CI: confidence interval.
[a]*P*-value indicates the comparison of AUCs between Radscore_whole and the other two signatures, respectively.
[b]*P*-value indicates the comparison of AUCs between Radscore_parenchyma and Radscore_mid-portion.

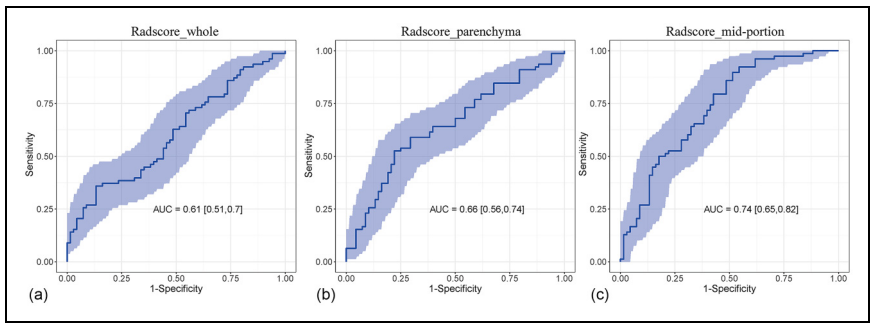


**Figure 2.** Bootstrap receiver operating characteristic (ROC) curves for various radiomics signatures. The blue shaded area represents the 95% confidence interval for the ROC, calculated through bootstrap sampling with 1000 replications.

radscore_mid-portion achieved sensitivity, specificity, and accuracy of 0.86, 0.51, and 0.70, respectively. The diagnostic performance of radscore_whole was comparable but slightly inferior to that of radscore_parenchyma (sensitivity, 0.69 vs 0.64; specificity, 0.46 vs 0.60; accuracy, 0.58 vs 0.62; AUC, 0.61 vs 0.66). The density map illustrates that the radscore_mid-portion provides clearer differentiation in assessing the severity of renal fibrosis compared to both the radscore_whole and radscore_parenchyma (Figure 3).

In the five-fold cross-validation, the diagnostic performance of the radscore_mid-portion remained robust, yielding an AUC of 0.74 (95% CI: 0.55–0.93), which also outperformed both the radscore_whole (AUC = 0.60, 95% CI: 0.39–0.81) and the radscore_parenchyma (AUC = 0.66, 95% CI: 0.45–0.86) (Figure 4).

### *Increment in performance of certain radiomics signature*

The radiomics signature obtained from the renal mid-portion region exhibited a notable improvement in discrimination accuracy, as presented in Table 4. It achieved an NRI value of 36.35% (95% CI: 4.44%–68.26%) and an IDI value of 10.57% (95% CI: 3.66%–17.48%) in comparison to the radiomics signature derived from the entire kidney region. Furthermore, when compared to the radiomics signature derived from the kidney parenchyma region, it demonstrated an NRI value of 42.23% (95% CI: 10.60%–73.86%) and an IDI value of 10.42% (95% CI: 3.36%–17.49%).

## Discussion

In the present study, we extracted radiomics features from different kidney regions on US images to construct region-specific radiomics signatures and evaluate their diagnostic efficacy. Our results showed that the radscore_mid-portion achieved superior performance in distinguishing moderate-to-severe fibrosis from mild fibrosis, surpassing both

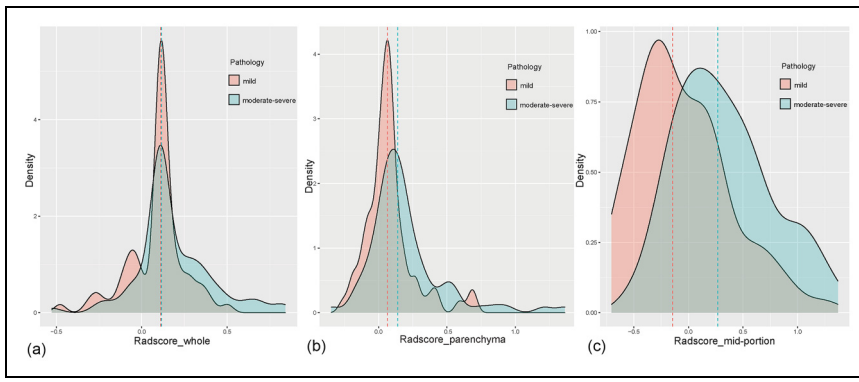


**Figure 3.** Density map illustrating extracted radiomics scores in mild versus moderate-to-severe renal fibrosis.

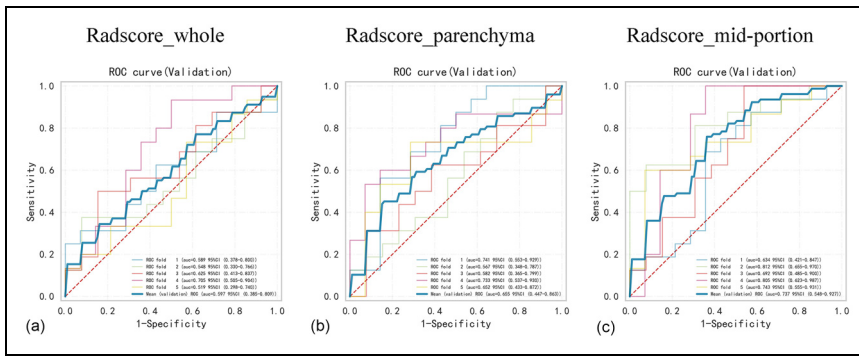


**Figure 4.** Receiver operating characteristic curves depicting the performance of different radiomics signatures in a five-fold cross-validation analysis.

**Table 4.** Performance improvement of radiomics signatures across varied regions.

| Index | NRI % (95% CI) | *P*-value | IDI % (95% CI) | *P*-value |
|---|---|---|---|---|
| Radscore_parenchyma versus Radscore_whole | 17.65 (−14.60–49.89) | 0.283 | 0.15 (−3.62–3.91) | 0.938 |
| Radscore_mid-portion versus Radscore_whole | 36.35 (4.44–68.26) | 0.025 | 10.57 (3.66–17.48) | 0.002 |
| Radscore_mid-portion versus Radscore_parenchyma | 42.23 (10.60–73.86) | 0.008 | 10.42 (3.36–17.49) | 0.003 |

NRI: net reclassification improvement; IDI: integrated discrimination improvement; CI: confidence interval.

radscore_whole and radscore_parenchyma. These findings highlight the renal mid-portion as the most informative region for radiomics-based assessment of renal fibrosis.

The radiomics approach yields a diverse array of quantitative image features extracted from US images, which cannot be recognized by human naked eyes. Several studies have highlighted notable progress in radiomics technology within the medical field, specifically in lesion diagnosis,[23] prognosis prediction,[24] and treatment efficacy assessment.[25] Presently, a multitude of researchers are actively investigating the applicability of radiomics techniques in nephropathy research. Recently, Bandara et al. utilized radiomics features extracted from the entire kidney region in US images, successfully distinguishing individuals with CKD from those in good health.[26] In another research, Ge et al. developed a radiomics nomogram that incorporated radiomics signature derived from the kidney parenchyma region in US images, demonstrating promising outcomes in stratifying the severity of renal fibrosis among CKD patients.[27] Meanwhile, Zhu et al. constructed machine learning models founded on radiomics features extracted from the mid-portion region of the kidney in US images, yielding satisfactory clinical utility for assessing transplant renal function.[28] It is evident that various researchers employ distinct approaches: some analyze the entire kidney region, others target kidney parenchyma for feature extraction, and a third group concentrates on the mid-portion of the kidney. Despite the favorable clinical outcomes observed in these studies, establishing a consensus regarding the optimal analysis region is paramount for the widespread acceptance and application of radiomics technology in nephropathy research.[29] Further research and standardization endeavors are imperative to address these discrepancies and augment the utility of radiomics in clinical practice.

This study developed three distinct radiomics signatures through the analysis of different renal regions: the entire kidney, renal parenchyma, and the mid-portion of the kidney. The results revealed that the radiomics signature originating from the mid-portion of the kidney demonstrated superior diagnostic performance, followed by those derived from the renal parenchyma. In contrast, the radiomics signature from the entire kidney exhibited the least favorable diagnostic efficacy. Renal fibrosis, a complex and progressive pathological condition, is often associated with various fibrotic changes in the renal parenchyma.[30] During the course of CKD, the extracellular matrix undergoes significant remodeling, leading to fibrotic tissue deposition in the affected kidney.[6] This underpins the theoretical basis for radiomics analysis aimed at assessing renal fibrosis severity through analyzing the renal parenchyma. However, when analyzing the entire kidney, the constructed radiomics signature exhibited the poorest diagnostic performance. This may be attributed to the inclusion of the kidney collecting system components in the analysis, which do not contribute to the renal fibrosis pathological process but introduce redundant information, hindering radiomics feature extraction and subsequent analysis. Furthermore, exclusive radiomics analysis of renal parenchyma demonstrated suboptimal diagnostic performance, potentially attributed to the vulnerability of imaging the kidney's upper and lower poles to issues such as edge shadowing or echo dropout caused by acoustic refraction.[31] Despite efforts to obtain the optimal renal US section during the examination, these factors ultimately undermined the sharpness and resolution of the image. Additionally, imaging quality of the renal parenchyma in the far field was compromised

due to acoustic attenuation, potentially contributing to the subpar diagnostic performance of the radiomics signature derived from renal parenchyma.[32] Undoubtedly, these factors would introduce confounding elements into the radiomics analysis process. In contrast, the central portion of the kidney, closest to the US probe's sound source, provided clearer images with minimal interference, facilitating effective radiomics feature extraction and enhancing diagnostic efficiency. Moreover, a previous study confirmed the feasibility of radiomics feature extraction from the renal mid-portion by demonstrating satisfactory intra-operator repeatability and inter-operator reproducibility.[33]

Moderate and severe renal fibrosis were analyzed together rather than as separate categories. The number of biopsy-confirmed severe fibrosis cases was extremely limited, consistent with previous epidemiological studies showing that advanced stages of CKD are relatively uncommon in the general population, with the prevalence of stage 4-5 CKD estimated to be below 0.3% worldwide.[1] In addition, patients with advanced disease are typically managed with dialysis or renal replacement therapy rather than undergoing renal biopsy, which further reduces the availability of histopathological specimens for severe fibrosis. From a clinical standpoint, patients with mild fibrosis are generally managed with conservative approaches aimed at slowing disease progression, whereas those with moderate or severe fibrosis require more intensive intervention, including closer follow-up and management of comorbid conditions.[3,4] Given the comparable therapeutic strategies for moderate and severe stages, merging them into a single analytical group was considered clinically relevant for the present analysis.

It should also be noted that although our findings indicated that the radiomics signature derived from the renal mid-portion achieved satisfactory diagnostic performance, the pathological reference standard was obtained from biopsy specimens of the lower pole. This anatomical discrepancy may raise concerns regarding potential sampling bias. However, the lower pole is conventionally selected for biopsy because of its safer access and reduced risk of vascular injury. Importantly, previous studies have demonstrated that in diffuse renal parenchymal diseases, histological indices, including the extent of interstitial fibrosis, global glomerulosclerosis, and glomerular yield, are broadly comparable between lower-pole and central cortical specimens.[34,35] These findings support the representativeness of lower-pole biopsies as a reference standard, thereby reinforcing the validity of our radiomics results. Moreover, this study provides an initial step toward advancing US radiomics for renal fibrosis assessment by identifying the most informative anatomical region. Establishing the renal mid-portion as the optimal site for feature extraction lays the groundwork for future clinical applications. Further developments may include automated segmentation software, integration of additional US parameters or clinical indicators, and the use of advanced artificial intelligence algorithms to build comprehensive diagnostic models. Importantly, the proposed approach relies on conventional B-mode US imaging that is already routinely available in clinical practice and therefore does not require specialized hardware. With continued validation and technical refinement, this strategy holds promise for facilitating non-invasive and widely applicable evaluation of renal fibrosis and may serve as a supportive tool to guide risk stratification and biopsy selection in clinical workflows.

While this study has made significant advancements, several limitations persist. First, the sample size is relatively small, necessitating future validation of the study's conclusions in a larger population cohort. Second, this is a single-center study, and external clinical validation

in collaboration with other hospitals will be necessary to confirm the generalizability of the findings in broader patient populations. Third, all renal US examinations were performed on a single system and probe. As radiomics features are known to be sensitive to acquisition parameters and system-specific characteristics, future studies across different US platforms, combined with harmonization techniques such as feature standardization or ComBat adjustment, will be essential to confirm the reproducibility and clinical applicability of our radiomics findings.

## Conclusion

Radiomics signatures derived from distinct renal regions on US images demonstrate varying diagnostic efficacy. The radiomics signature established within the renal midportion region presents considerable advantages over those derived from either the entire kidney or kidney parenchyma regions. These findings hold promise for the enhancement and refinement of the radiomics analysis framework for renal US, thereby advancing the field of nephropathy research.

### Acknowledgements

The authors thank Zhongzhen Su for valuable guidance in the study design.

### Ethical approval

The study was conducted according to the Declaration of Helsinki guidelines, and approved by the Institutional Review Board (or Ethics Committee) of the Fifth Affiliated Hospital of Sun Yat-sen University (protocol code: K09-1; approval date: May 2019).

### Author contributions

Conception and design: Ziman Chen.
Administrative support: Ziman Chen.
Provision of study materials or patients: Ziman Chen, Chaoqun Wu.
Collection and assembly of data: Ziman Chen, Yingli Wang, Chaoqun Wu.
Data analysis and interpretation: Ziman Chen.
Manuscript writing: Ziman Chen.
Final approval of manuscript: All authors.

### Funding

The authors disclosed receipt of the following financial support for the research, authorship, and/or publication of this article: This work was supported by the Hong Kong Polytechnic University (grant number P0056738).

### Declaration of conflicting interests

The authors declared no potential conflicts of interest with respect to the research, authorship, and/or publication of this article.

## Data availability

The data presented in this study are available on reasonable request from the corresponding author. The data are not publicly available due to ethical concerns regarding privacy.

## Supplemental material

Supplemental material for this article is available online.

## ORCID iD

Ziman Chen https://orcid.org/0000-0002-2765-5002

## References

1. Collaboration GBDCKD. Global, regional, and national burden of chronic kidney disease, 1990–2017: a systematic analysis for the Global Burden of Disease Study 2017. *Lancet* 2020; 395: 709–733.
2. Zhang L, Zhao MH, Zuo L, et al. China Kidney Disease Network (CK-NET) 2016 annual data report. *Kidney Int Suppl* 2011; 10: e97–e185.
3. Meguid El Nahas A and Bello AK. Chronic kidney disease: the global challenge. *Lancet* 2005; 365: 331–340.
4. Kalantar-Zadeh K and Li PK. Strategies to prevent kidney disease and its progression. *Nat Rev Nephrol* 2020; 16: 129–130.
5. Panizo S, Martinez-Arias L, Alonso-Montes C, et al. Fibrosis in chronic kidney disease: Pathogenesis and consequences. *Int J Mol Sci* 2021; 22: 408.
6. Ruiz-Ortega M, Rayego-Mateos S, Lamas S, et al. Targeting the progression of chronic kidney disease. *Nat Rev Nephrol* 2020; 16: 269–288.
7. Hogan JJ, Mocanu M and Berns JS. The native kidney biopsy: update and evidence for best practice. *Clin J Am Soc Nephrol* 2016; 11: 354–362.
8. Halimi JM, Gatault P, Longuet H, et al. Major bleeding and risk of death after percutaneous native kidney biopsies: a French nationwide cohort study. *Clin J Am Soc Nephrol* 2020; 15: 1587–1594.
9. Singla RK, Kadatz M, Rohling R, et al. Kidney ultrasound for nephrologists: a review. *Kidney Med* 2022; 4: 100464.
10. Lucisano G, Comi N, Pelagi E, et al. Can renal sonography be a reliable diagnostic tool in the assessment of chronic kidney disease? *J Ultrasound Med* 2015; 34: 299–306.
11. Yaprak M, Cakir O, Turan MN, et al. Role of ultrasonographic chronic kidney disease score in the assessment of chronic kidney disease. *Int Urol Nephrol* 2017; 49: 123–131.
12. Liang X, Du M and Chen Z. Artificial intelligence-aided ultrasound in renal diseases: a systematic review. *Quant Imaging Med Surg* 2023; 13: 3988–4001.
13. Song KD. Current status of deep learning applications in abdominal ultrasonography. *Ultrasonography* 2021; 40: 177–182.
14. Park SH. Artificial intelligence for ultrasonography: unique opportunities and challenges. *Ultrasonography* 2021; 40: –6.
15. Liu Z, Wang S, Dong D, et al. The applications of radiomics in precision diagnosis and treatment of oncology: opportunities and challenges. *Theranostics* 2019; 9: 1303–1322.

16. Zwanenburg A, Vallieres M, Abdalah MA, et al. The image biomarker standardization initiative: standardized quantitative radiomics for high-throughput image-based phenotyping. *Radiology* 2020; 295: 328–338.
17. Qin X, Xia L, Zhu C, et al. Noninvasive evaluation of lupus nephritis activity using a radiomics machine learning model based on ultrasound. *J Inflamm Res* 2023; 16: 433–441.
18. Iqbal F, Pallewatte AS and Wansapura JP. Texture analysis of ultrasound images of chronic kidney disease. 2017 Seventeenth International Conference on Advances in ICT for Emerging Regions (ICTer), 2017, pp. 1–5.
19. Guo S, Huang X, Xu C, et al. Multiregional radiomic model for breast cancer diagnosis: value of ultrasound-based peritumoral and parenchymal radiomics. *Quant Imaging Med Surg* 2023; 13: 3127–3139.
20. Stevens PE and Levin A. Kidney disease: improving global outcomes chronic kidney disease guideline development work group M. Evaluation and management of chronic kidney disease: synopsis of the kidney disease: improving global outcomes 2012 clinical practice guideline. *Ann Intern Med* 2013; 158: 825–830.
21. von Elm E, Altman DG, Egger M, et al. The Strengthening the Reporting of Observational Studies in Epidemiology (STROBE) statement: guidelines for reporting observational studies. *Ann Intern Med* 2007; 147: 573–577.
22. Chen Z, Chen J, Chen H, et al. Evaluation of renal fibrosis in patients with chronic kidney disease by shear wave elastography: a comparative analysis with pathological findings. *Abdom Radiol (NY)* 2022; 47: 738–745.
23. Peng Y, Lin P, Wu L, et al. Ultrasound-based radiomics analysis for preoperatively predicting different histopathological subtypes of primary liver cancer. *Front Oncol* 2020; 10: 1646.
24. Jin J, Yao Z, Zhang T, et al. Deep learning radiomics model accurately predicts hepatocellular carcinoma occurrence in chronic hepatitis B patients: a five-year follow-up. *Am J Cancer Res* 2021; 11: 576–589.
25. Jiang M, Li CL, Luo XM, et al. Ultrasound-based deep learning radiomics in the assessment of pathological complete response to neoadjuvant chemotherapy in locally advanced breast cancer. *Eur J Cancer* 2021; 147: 95–105.
26. Bandara MS, Gurunayaka B, Lakraj G, et al. Ultrasound based radiomics features of chronic kidney disease. *Acad Radiol* 2022; 29: 229–235.
27. Ge XY, Lan ZK, Lan QQ, et al. Diagnostic accuracy of ultrasound-based multimodal radiomics modeling for fibrosis detection in chronic kidney disease. *Eur Radiol* 2023; 33: 2386–2398.
28. Zhu L, Huang R, Li M, et al. Machine learning-based ultrasound radiomics for evaluating the function of transplanted kidneys. *Ultrasound Med Biol* 2022; 48: 1441–1452.
29. van Timmeren JE, Cester D, Tanadini-Lang S, et al. Radiomics in medical imaging-"how-to" guide and critical reflection. *Insights Imaging* 2020; 11: 91.
30. Humphreys BD. Mechanisms of renal fibrosis. *Annu Rev Physiol* 2018; 80: 309–326.
31. Naganuma H, Ishida H, Uno A, et al. Refraction artifact on abdominal sonogram. *J Med Ultrason (2001)* 2021; 48: 273–283.
32. Case TD. Ultrasound physics and instrumentation. *Surg Clin North Am* 1998; 78: 197–217.
33. Chen Z, Ying MTC, Wang Y, et al. Ultrasound-based radiomics analysis in the assessment of renal fibrosis in patients with chronic kidney disease. *Abdom Radiol (NY)* 2023; 48: 2649–2657.

34. Gerth J, Busch M, Illner N, et al. Are tissue samples from two different anatomical areas of the kidney necessary for adequate diagnosis? *Clin Nephrol* 2010; 74: 258–265.
35. Peters B, Molne J, Hadimeri H, et al. Sixteen Gauge biopsy needles are better and safer than 18 Gauge in native and transplant kidney biopsies. *Acta Radiol* 2017; 58: 240–248.